CrossMark

ORIGINAL PAPER

A Facile Method to Synthesize Nickel Ferrite Nanoparticles: Parameter Effect

Oznur Karaagac[1] · Suheda Atmaca[1] · Hakan Kockar[1]

Abstract Nickel ferrite nanoparticles were synthesized by co-precipitation/hydrothermal synthesis. The synthesis temperature of the co-precipitation of the precursor was studied. At this stage, proper reaction temperature to synthesize superparamagnetic nickel ferrite nanoparticles with zero coercivity (H_c) was found to be 80 °C. More importantly, the effects of temperature and time of the hydrothermal process on the structural and magnetic properties of the nanoparticles were also investigated. X-ray diffraction (XRD) and Fourier transform infrared spectroscopy were used for the structural analysis. Particle sizes and shapes were determined by transmission electron microscopy (TEM). Magnetic measurements were done by using a vibrating sample magnetometer (VSM). The particle sizes d_{XRD}, d_{TEM} and d_{VSM} of nickel ferrite nanoparticles were calculated from XRD patterns, TEM images and magnetic data, respectively. By hydrothermal process, the reaction time is seen to be effective on the properties of $NiFe_2O_4$ nanoparticles since the size of the nanoparticles and saturation magnetization (M_s) increase with the increase of the time. The effect of reaction temperature on the properties of nickel ferrite nanoparticles is also slightly observed. It is seen that the synthesized nanoparticles at 125 °C for 40 h exhibit a superparamagnetic behaviour (zero H_c). And M_s is found to be 50.8 emu/g which is a substantially high value. Also, the limit of superparamagnetic particle size for our study is ∼12 nm since $NiFe_2O_4$ nanoparticles bigger than 12 nm show H_c.

✉ Oznur Karaagac
  karaagac@balikesir.edu.tr

[1] Physics Department, Science and Literature Faculty, Balikesir University, 10145, Cagis, Balikesir, Turkey

1 Introduction

Ferrite nanoparticles (MFe_2O_4, M = Fe, Ni, Co, Mn, etc.) have various applications in magnetic films [1], magnetic fluids [2], catalysis [3], magnetic resonance imaging (MRI) [4, 5], magnetic hyperthermia [2, 5] and drug delivery [6, 7]. Also, nickel ferrite ($NiFe_2O_4$) nanoparticles have promising electrical and magnetic properties and are frequently used in electronic devices [8], high frequency applications [9], MRI contrast agents [10], etc. Magnetic nanoparticles can be synthesized by various techniques including co-precipitation, hydrothermal synthesis, thermal decomposition, microemulsion and sol-gel [11, 12]. The co-precipitation is a simple and efficient way to synthesize high-yield magnetic nanoparticles [13]. However, a co-precipitation method cannot solely be used to prepare $NiFe_2O_4$ nanoparticles without further processes, such as hydrothermal process [14], annealing [15] and calcination [16].

In the study [16], nickel ferrite nanoparticles are synthesized by a co-precipitation/calcination process. In the first step, FeOOH and $Ni(OH)_2$ are obtained as a precursor and the precursor is calcinated at high temperatures (650 and 800 °C) for 2 h in air environment. The $NiFe_2O_4$ nanoparticles obtained in this study show coercivity (H_c), and their saturation magnetization (M_s) values are 33 and 49 emu/g. In another study [15], $NiFe_2O_4$ nanoparticles are co-precipitated in the first step and annealed afterwards. The obtained nanoparticles are 17 nm in size. The M_s of the sample is 44 emu/g and its H_c is 51 Oe. Wang et al. [14]

Table 1 Synthesis conditions of the precursor, particle sizes and magnetic properties of the final product $NiFe_2O_4$ nanoparticles

Sample	Temperature (°C)	Particle sizes			Magnetic properties		
		d_{TEM} (nm $\pm$ Δnm)	d_{XRD} (nm)	d_{VSM} (nm $\pm$ Δnm)	M_s (emu/g)	H_c (Oe)	Magnetic state
A1	20	134 ± 35	52.6	–	1.1^a	36	Paramagnetic with a slight ferromagnetic effect
A2	40	12.3 ± 5.0	16.3	–	54.4	4	SP with 4 Oe
A3	60	15.5 ± 5.8	19.3	–	54.3	2	SP with 2 Oe
$A4^b$	80	10.1 ± 3.6	10.6	6.9 ± 0.6	48.7	–	SP

SP superparamagnetic

[a] M_s value is the maximum magnetization at the highest applied magnetic field for sample A1

[b] A4 is the same sample with B2 and B7

obtained a colloidal suspension by co-precipitation in the first step, and this suspension is hydrothermally processed at 180 °C for 6–48 h. $NiFe_2O_4$ nanoparticles obtained in the co-precipitation/hydrothermal synthesis show H_c. Superparamagnetic $NiFe_2O_4$ nanoparticles are also obtained in [17]; however, the M_s values are highly low. Barreto et al. [17] obtained superparamagnetic $NiFe_2O_4$ nanoparticles by the co-precipitation/calcination process. The M_s values of the nanoparticles are as low as 13 and 15 emu/g. In [18], $NiFe_2O_4$ nanoparticles are synthesized hydrothermally with and without using surfactants. The M_s values of the sample with zero H_c is around 35 emu/g, and the sample with higher M_s ($\sim$40 emu/g) shows H_c ($\sim$17 Oe).

In the synthesis of $NiFe_2O_4$ nanoparticles, Albuquerque et al. [8] and Shi et al. [19] proposed that co-precipitation only produces the amorphous precursor for the synthesis of $NiFe_2O_4$ in the second step. Furthermore, Shi et al. [19] regarded the precursor phase as hydroxide. It is known that hydrothermal synthesis allows controlling the particle size and crystallinity through the reaction time and temperature [20]. Thus, hydrothermal synthesis as a second step provides $NiFe_2O_4$ formation with controlling the particle size and crystallinity through the reaction time and temperature. In this study, $NiFe_2O_4$ nanoparticles are synthesized in a two-step co-precipitation/hydrothermal process. The effect of the temperature on the co-precipitation is investigated to determine the proper temperature. In the second step, the effects of the temperature and time are studied. The structural and magnetic properties of the final product are investigated. Superparamagnetic $NiFe_2O_4$ nanoparticles with a quite high M_s value of 50.8 emu/g, which is close to the M_s value of bulk $NiFe_2O_4$, are obtained.

2 Experimental

$NiCl_2 \cdot 6H_2O$ (Riedel-de Haën, > 97 %), $FeCl_3 \cdot 6H_2O$ (Sigma-Aldrich, > 99 %) and NH_4OH (Merck, 25 % of
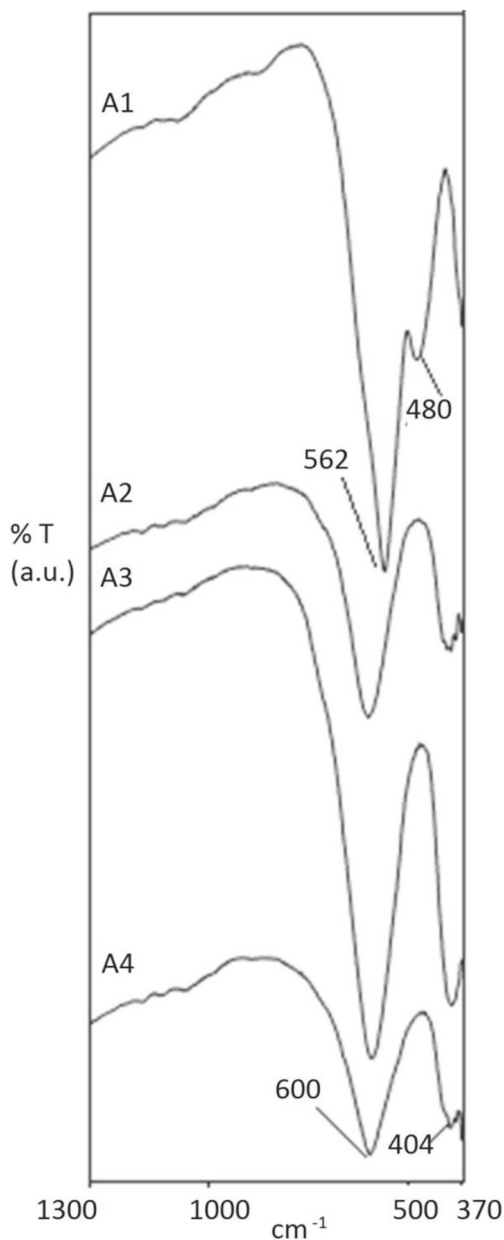
Fig. 1 XRD patterns of samples A1, A2, A3 and A4
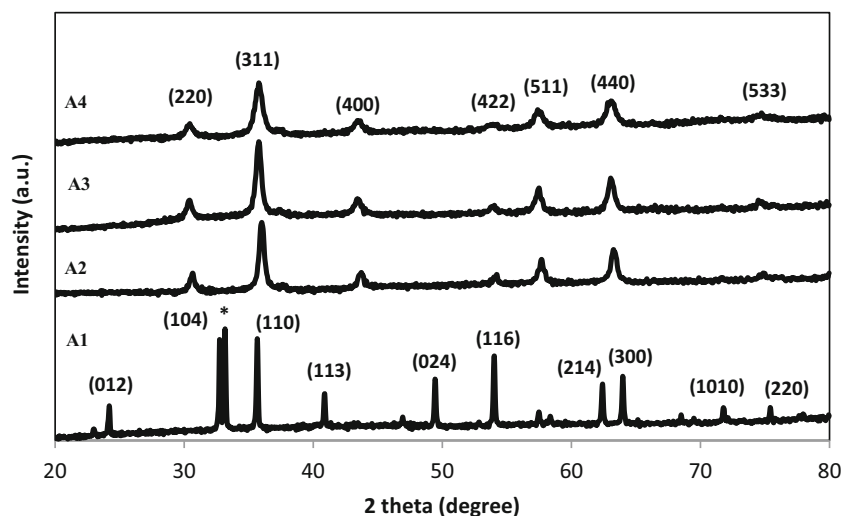
ammonia) were used in this work. All reagents were of analytical grade and used without further purification. For the first step, the co-precipitation process, the precursor was synthesized under air atmosphere. Ni^{2+} and Fe^{3+} were dissolved with a 1:2 molar ratio in 25 ml deionized water. Then, 25 ml NH_4OH was added into solution under vigorous stirring. The solution was stirred at 1000 rpm for 45 min. For the second step, the hydrothermal process, 15 ml of the precursor was transferred into a Teflon-lined stainless

Fig. 2 FT-IR spectrum of samples A1, A2, A3 and A4

steel autoclave. The sealed autoclave was put into an oven, and the reaction temperature was changed between 125 and 200 °C for 40 h to reveal the temperature effect. And the reaction was performed at 150 °C for 10–80 h in order to investigate the effect of the reaction time on the properties of the nanoparticles. When the reaction was completed, the autoclave cooled down to room temperature naturally and the resulting black precipitate was washed with deionized water several times and dried in oven at 60 °C.

The crystal structure of the samples was characterized by the X-ray diffraction (XRD) technique, using a PANalytical's X'Pert Pro X-ray diffractometer. Scan was performed between 20° and 80° by using CuK_α radiation (λ = 1.54056 Å). Fourier transform infrared spectroscopy (FT-IR, PerkinElmer) was used to obtain the transmittance spectrum of the samples at a 370–4000 cm^{-1} range using KBr pellets. Transmission electron microscopy (TEM) images were taken by using a FEI Tecnai G2 F30 model high-resolution microscope. The samples were prepared by placing a drop of the diluted suspension of the samples on a carbon-coated copper grid. ImageJ programme was used to calculate the particle sizes after taking the TEM pictures of nanoparticles. The magnetic properties were investigated using a ADE EV9 model vibrating sample magnetometer (VSM) at room temperature between −20 and +20 kOe by 1-Oe intervals.

3 Results and Discussion

In order to obtain the precursor of the hydrothermal process, the first-step reactions were performed at different temperatures (20, 40, 60 and 80 °C) and the effect of the temperature on the properties of the final product was investigated. Synthesis conditions and structural and magnetic properties of the samples are given in Table 1. The precursor of sample A1 was obtained at 20 °C, and the sample was hydrothermally synthesized at 150 °C for 40 h afterwards. For the other samples (A2, A3 and A4), the precursors were obtained at 40, 60 and 80 °C, respectively, and the samples were synthesized at the same conditions as A1 in the hydrothermal step. The XRD pattern of sample A1 includes the peaks of crystal planes (012), (104), (110), (113), (024), (116), (214), (300), (1010) and (220) at 2θ = 24.2°, 32.7°, 36.7°, 40.9°, 49.4°, 54.0°, 62.4°, 64.0°, 71.8° and 75.4°, respectively (Fig. 1). These peaks correspond to hematite (JCPDS no. 33-0664). The peak (labelled with asterisk) observed at 33.2°, near the (104) peak of hematite, may correspond to ferrihydrite (JCPDS no. 46-1315). The intense peaks were only labelled, and the rest seems to belong to hematite and/or iron oxide hydroxide phases according

to the JCPDS card nos. 33-0664, 46-1315, 76-2301 and 89-6096. All these peaks imply that the sample is mainly hematite. It is known that iron oxide hydroxide converts to hematite by thermal transformation [21]. In our case, sample A1 is mainly hematite according to the structural analysis and magnetic measurements showing a low magnetization value (see Table 1). Black precipitate of $NiFe_2O_4$ was obtained at 40, 60 and 80 °C. In the XRD pattern of sample A2 in Fig. 1, (220), (311), (400), (422), (511), (440) and (533) peaks are observed at $2\theta = 30.7°$, 36.1°, 43.7°, 54.2°, 57.7°, 63.4° and 74.9°, respectively. The same peaks are seen in the XRD patterns of samples A3 and A4.

The observed peaks are the characteristic peaks of $NiFe_2O_4$ according to the JCPDS card no. 86-2267. The mean crystal sizes, d_{XRD}, were calculated from the most intense peaks of the main phase in the patterns using the Scherrer equation [22], and the results are given in Table 1. The d_{XRD} of sample A1 is 52.6 nm. The d_{XRD} of samples A2, A3 and A4 is 16.3, 19.3 and 10.6 nm, respectively.

For further information about the structure of the samples, FT-IR analysis was done and the spectra of all samples are shown in the 1300–370 cm^{-1} region in Fig. 2. Two main metal-oxygen bands are seen in the FT-IR spectra. The highest band, observed at $\nu_1 = 600$–550 cm^{-1}, corresponds
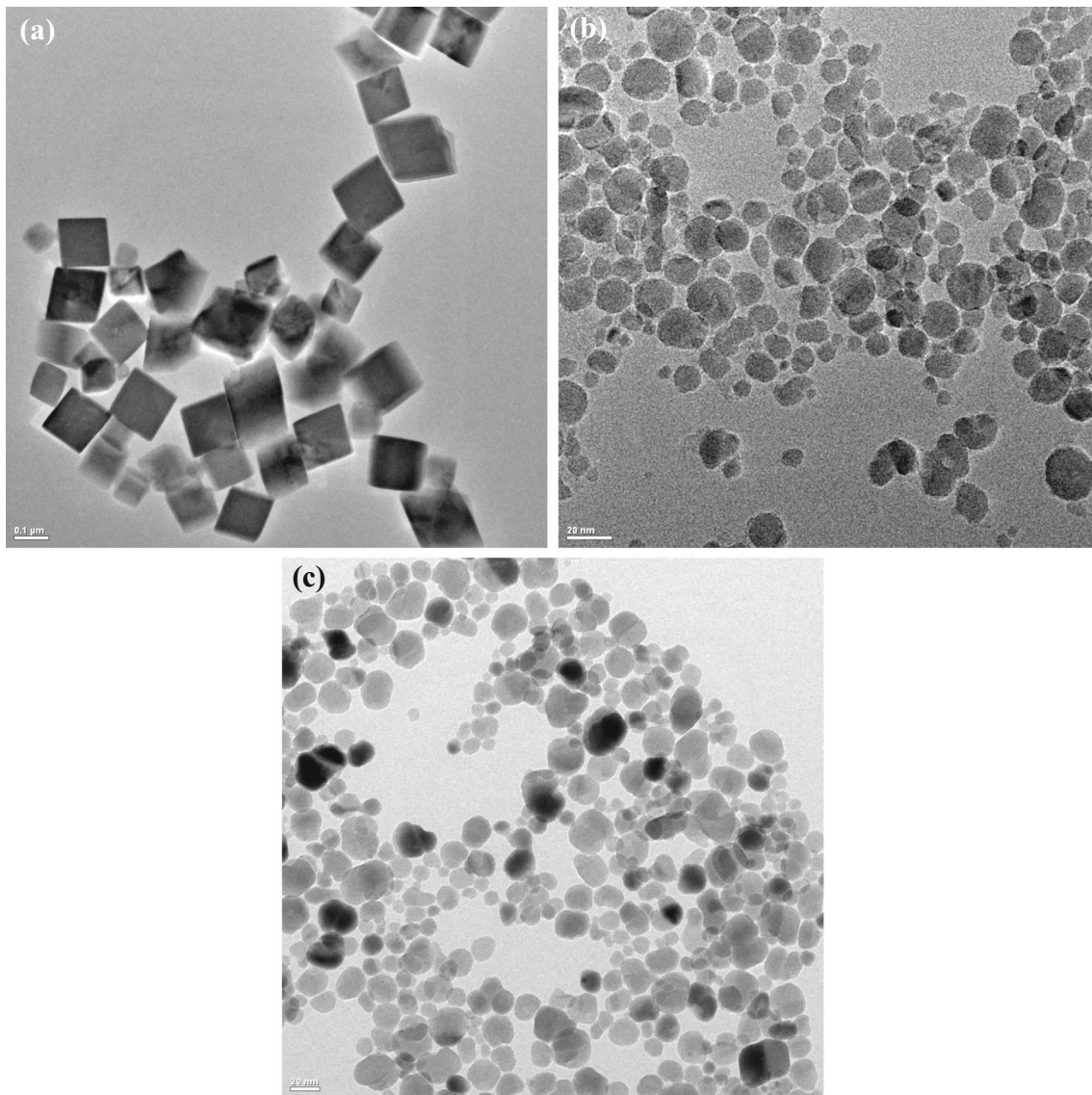

Fig. 3 TEM images of samples **a** A1, **b** A2 and **c** A3 (*scale bar* is 100 nm for A1 and 20 nm for A2 and A3)

to intrinsic stretching vibrations of the metal at the tetrahedral site (M_{tetr}-O), whereas the lowest band at $\nu_2 = 450$–385 cm^{-1} is assigned to octahedral metal stretching vibration (M_{oct}-O) [18, 23]. In the spectrum of A1, the bands observed at 480 and 562 cm^{-1} imply that the sample

is hematite [24]. The transmittance bands of samples A2, A3 and A4 are observed at about 404 and 600 cm^{-1}, indicating that the samples are $NiFe_2O_4$ [18, 25].

TEM images of the samples (A1–A3) are given in Fig. 3. As can be seen from Fig. 3a, sample A1 has cubic particles

Fig. 4 Magnetization curves of samples **a** A1 and **b** A2–A4. *Inset* shows the curves at ± 100 Oe
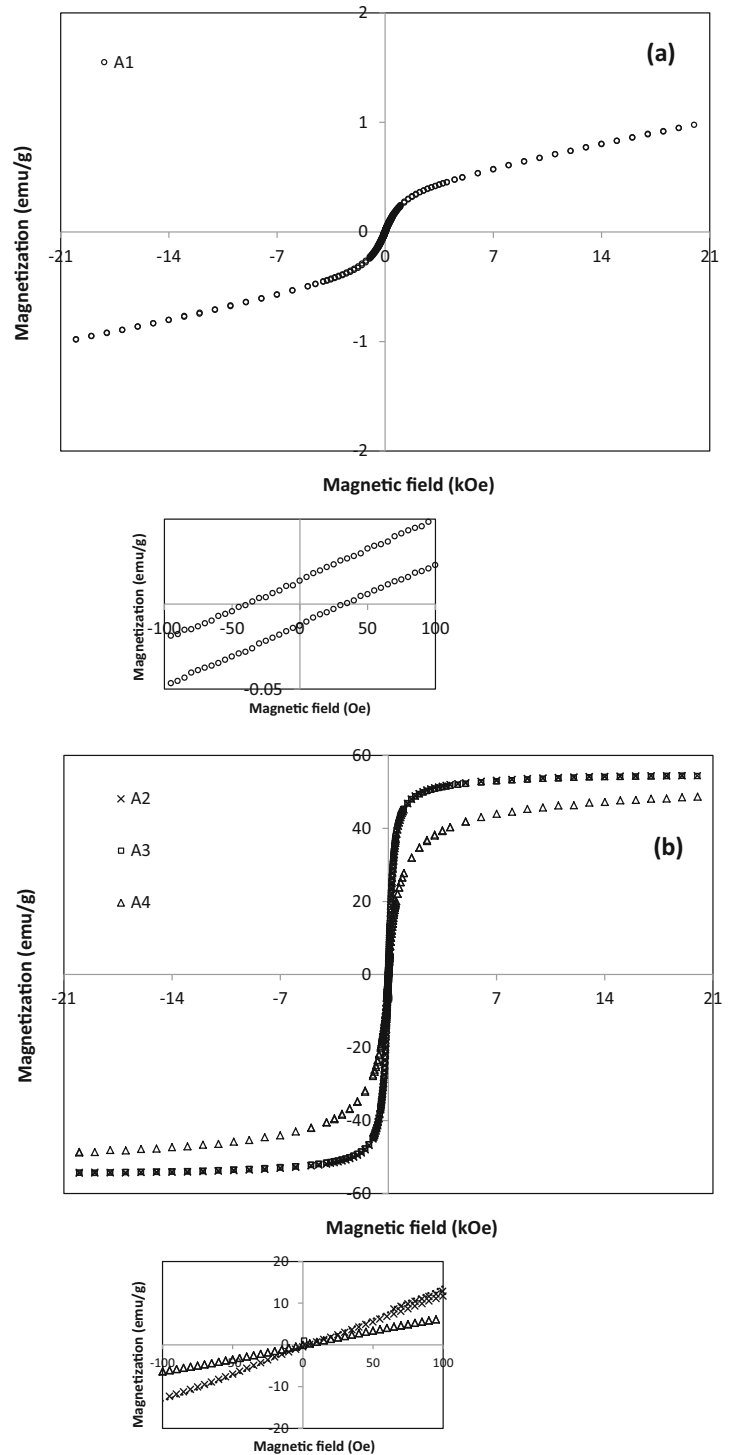
Table 2 Synthesis conditions, particle sizes and magnetic properties of NiFe$_2$O$_4$ nanoparticles

| Sample	Reaction temperature (°C)	Reaction time (h)	Particle sizes			Magnetic properties		
			d_{TEM} (nm $\pm$ Δnm)	d_{XRD} (nm)	d_{VSM} (nm $\pm$ Δnm)	M_s (emu/g)	H_c (Oe)	Magnetic state
B1	125	40	–	12.5	8.0 $\pm$ 0.4	50.8	–	SP
B2	150	40	10.1 $\pm$ 3.6	10.6	6.9 $\pm$ 0.6	48.7	–	SP
B3	175	40	–	–	7.3 $\pm$ 0.5	49.5	–	SP
B4	200	40	11.4 $\pm$ 3.8	12.5	7.4 $\pm$ 0.5	48.5	–	SP
B5	150	10	6.6 $\pm$ 2.9	7.9	6.7 $\pm$ 0.6	45.6	–	SP
B6	150	20	–	–	7.1 $\pm$ 0.5	48.2	–	SP
B7 (B2)	150	40	10.1 $\pm$ 3.6	10.6	6.9 $\pm$ 0.6	48.7	–	SP
B8	150	60	–	–	6.8 $\pm$ 0.6	48.9	–	SP
B9	150	80	11.9 $\pm$ 3.9	11.8	–	51.7	2	SP with 2 Oe

with high particle size. In the images of samples A2 and A3, nanoparticles are roundish and particle size distribution is wider. The physical particle sizes, d_{TEM}, of samples A1, A2, A3 and A4 are 134 $\pm$ 35, 12.3 $\pm$ 5.0, 15.5 $\pm$ 5.8 and 10.1 $\pm$ 3.6 nm, respectively, and are given in Table 1. It is observed that the calculated d_{TEM} value of A1 is bigger than the d_{XRD} value. This difference can be explained by considering that the particles are polycrystalline and the particle size is not equal to crystallite size. The d_{TEM} of the other samples shows the same trend with d_{XRD} as the temperature changes.

The magnetization curves of the nanoparticles (A1–A4) are presented in Fig. 4. Insets show the curves at $\pm$ 100

Oe. As seen from Fig. 4a, sample A1 is almost paramagnetic with a little ferromagnetic contribution. The maximum magnetization value (maximum magnetization measured at the highest applied magnetic field) of the sample is 1.1 emu/g and coercivity (H_c) is 36 Oe. Samples A2 and A3 are superparamagnetic with 4 and 2 Oe H_c, respectively. And their saturation magnetizations (M_s) are 54.4 and 54.3 emu/g, respectively. Sample A4 is superparamagnetic with zero H_c, and the M_s is 48.7 emu/g. The mean magnetic size, d_{MAG}, of the sample with zero H_c was calculated according to the equation in [26] and found to be 6.9 $\pm$ 0.6 nm (see Table 1).
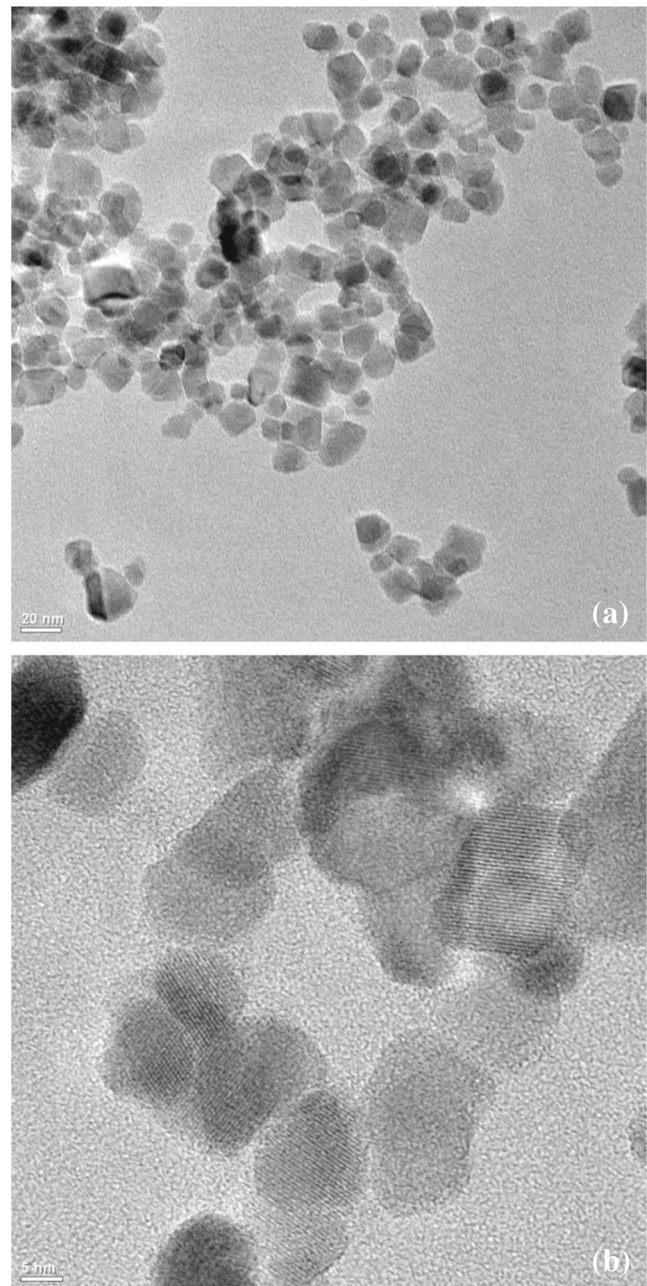

Fig. 5 XRD patterns of the nanoparticles synthesized at different temperatures (*B1* 125 °C, *B2* 150 °C and *B4* 200 °C)
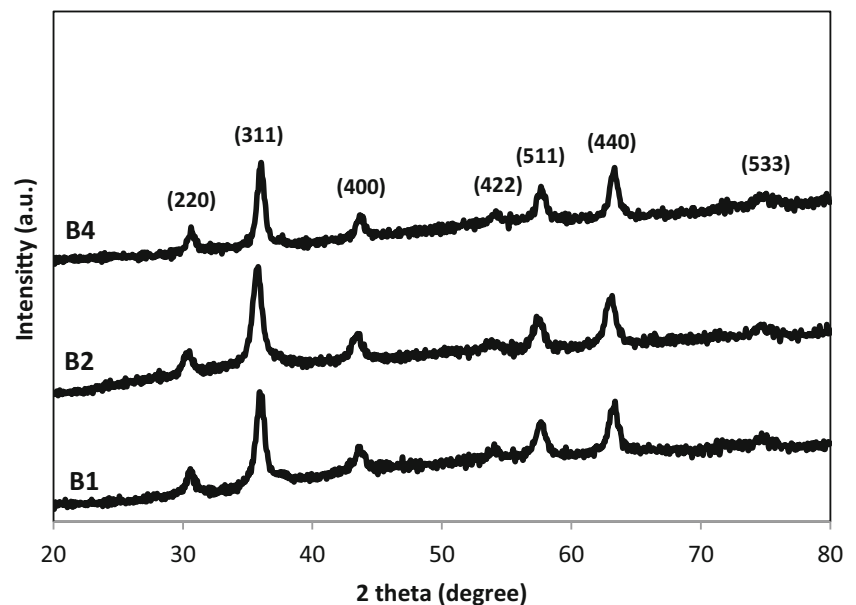
In order to investigate the effect of reaction temperature and time of the hydrothermal process on the structural and magnetic properties of the samples, the temperature was changed from 125 to 200 °C and the time was increased from 10 to 80 h, separately. The precursors of all these samples were obtained at 80 °C. Samples B1–B4 were synthesized at different temperatures, and samples B5–B9 were synthesized at different times by using the same precursor. The samples and synthesis conditions are given in Table 2. XRD patterns of samples B1, B2 and B4 synthesized at different temperatures (125, 150 and 200 °C, respectively) are given in Fig. 5. The (220), (311), (400), (422), (511), (440) and (533) peaks of the $NiFe_2O_4$ are observed in the patterns at $2\theta = 30.5°$, 35.9°, 43.7°, 54.1°, 57.6°, 63.4° and 74.7°, respectively. The d_{XRD} was calculated from the (311) peak in the patterns, and the results are given in Table 2 as 12.5, 10.6 and 12.5 nm for B1, B2 and B4, respectively. The particle sizes obtained from XRD patterns slightly fluctuate with the change of reaction temperature.
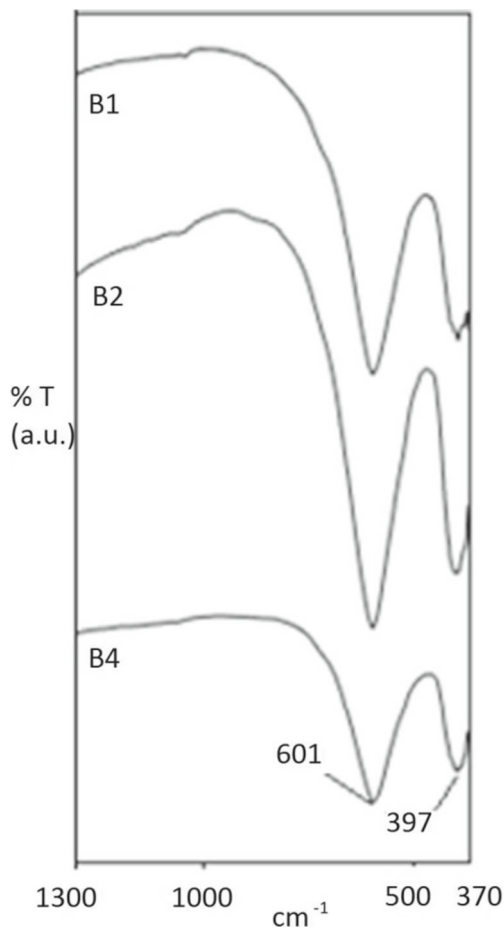
According to the FT-IR spectrum in Fig. 6, the samples (B1, B2, B4) are $NiFe_2O_4$. All samples in the spectrum show the characteristic bands at around 397 and 601 cm^{-1}. TEM images of sample B4 in 20- and 5-nm scales are given in Fig. 7a, b, respectively. The d_{TEM} of the samples calculated from the images is 10.1 ± 3.6 and 11.4 ± 3.8 nm for B2 and B4, respectively. Magnetization curves of the

Fig. 6 FT-IR spectrum of the nanoparticles synthesized at different temperatures (*B1* 125 °C, *B2* 150 °C and *B4* 200 °C)

Fig. 7 TEM images of the nanoparticles synthesized at 200 °C (B4) in **a** 20-nm scale and **b** 5-nm scale

Fig. 8 Magnetization curves of the nanoparticles synthesized at different temperatures (*B1* 125 °C, *B2* 150 °C, *B3* 175 °C and *B4* 200 °C). *Inset* shows the curves at ± 100 Oe
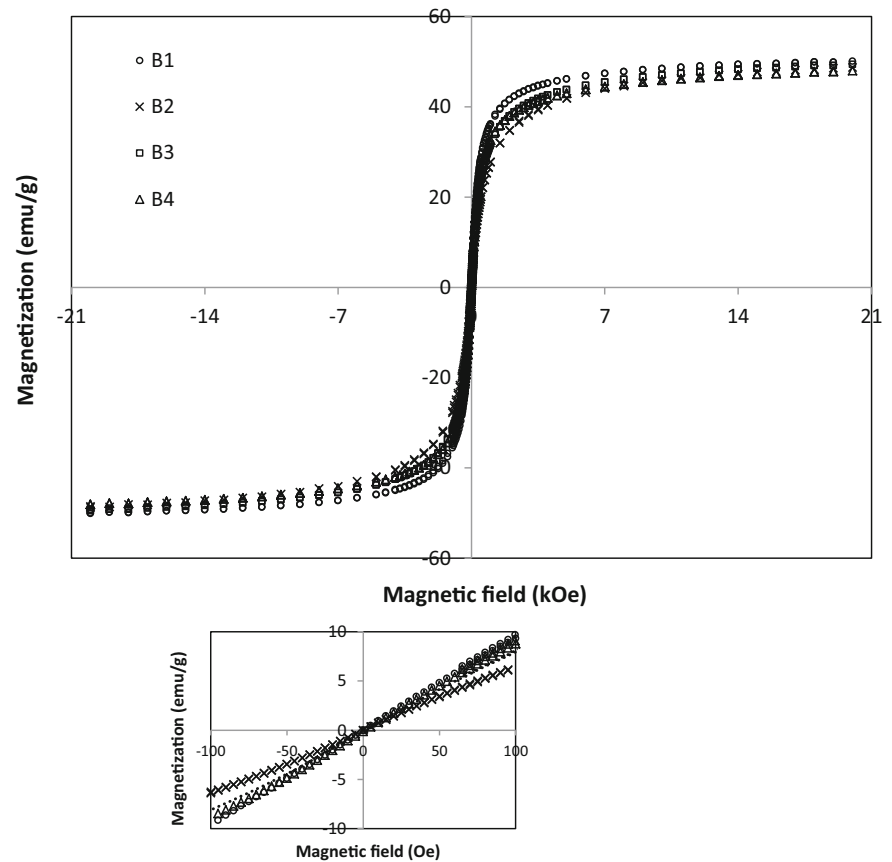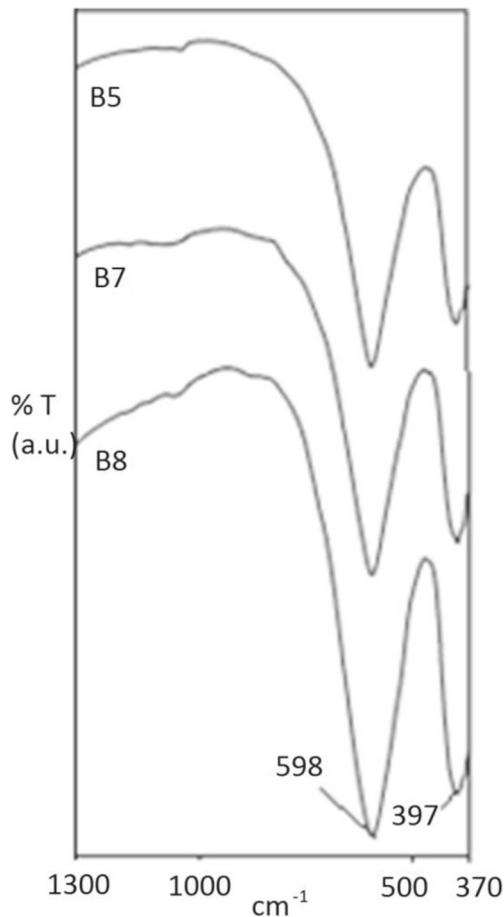

nanoparticles synthesized at different temperatures are presented in Fig. 8. All samples are superparamagnetic with zero H_c. M_s values of samples B1–B4 are 50.8, 48.7, 49.5 and 48.5 emu/g, respectively. M_s slightly changes according

to the reaction temperature. In [16], NiFe$_2$O$_4$ nanoparticles synthesized by the co-precipitation/calcination process are ferrimagnetic, showing 33 and 49 emu/g M_s. In another study [15], NiFe$_2$O$_4$ nanoparticles are obtained by

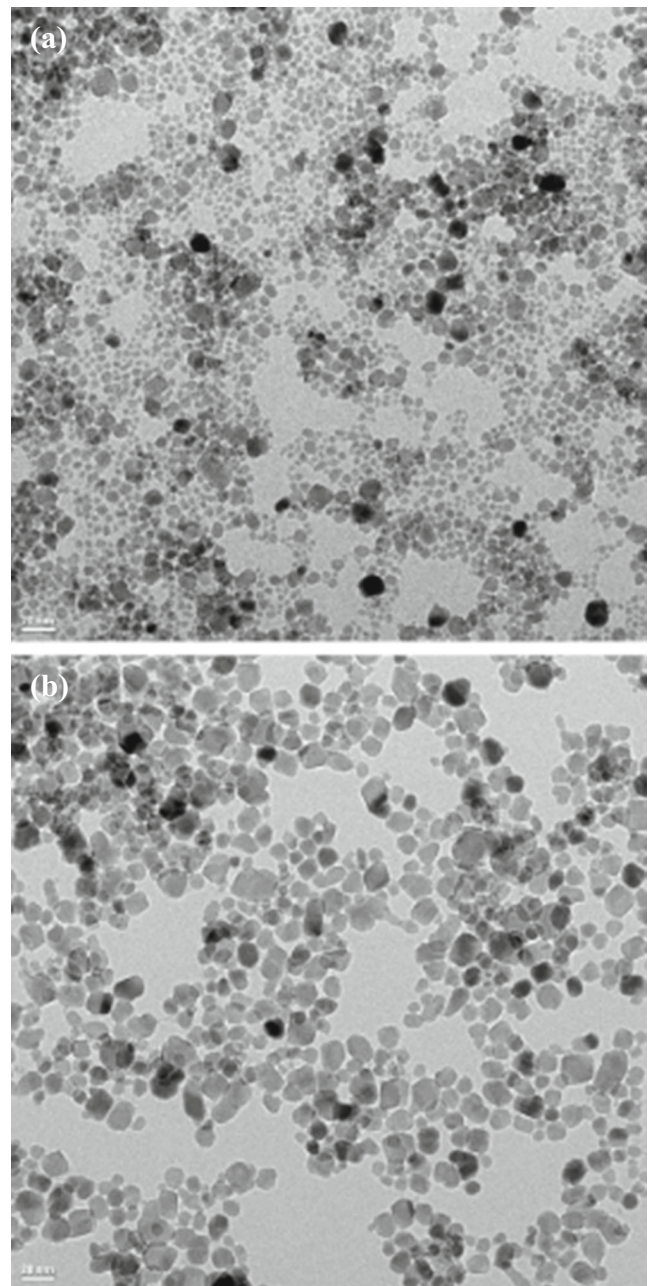**Fig. 9** XRD patterns of the nanoparticles synthesized at different times (*B5* 10 h, *B7* 40 h and *B9* 80 h)
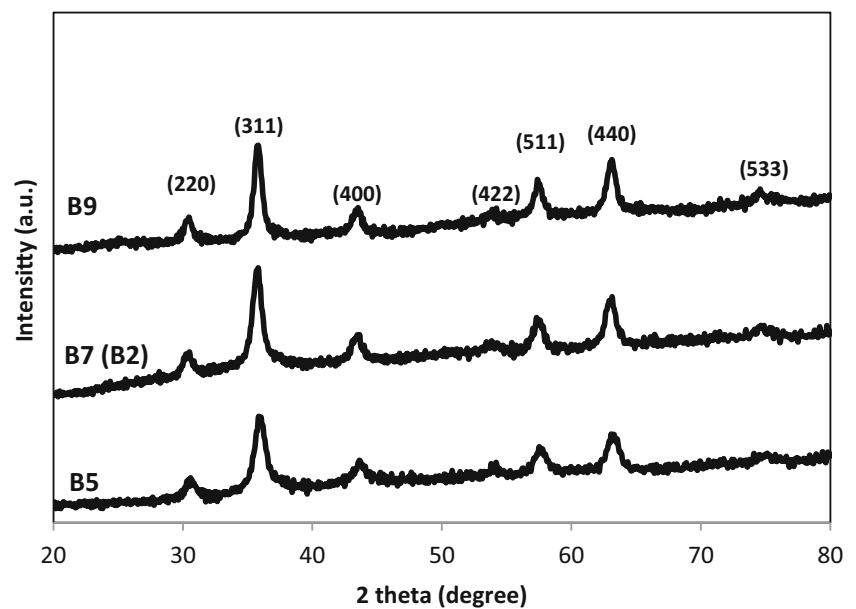
Fig. 10 FT-IR spectrum of the nanoparticles synthesized at different times (*B5* 10 h, *B7* 40 h and *B8* 60 h)

co-precipitation/annealing and the nanoparticles (17 nm) are ferrimagnetic with $M_s = 44$ emu/g and $H_c = 51$ Oe. $NiFe_2O_4$ nanoparticles synthesized solvothermally in the study of Wang et al. [14] show high M_s values between 37.7 and 53.3 emu/g; however, they show H_c from 41.8 to 58.2 Oe. Superparamagnetic $NiFe_2O_4$ nanoparticles are also obtained in [17] by the co-precipitation/calcination process; however, the M_s values are highly low as 13 and 15 emu/g. In another study [18], hydrothermally synthesized $NiFe_2O_4$ nanoparticles show two kinds of magnetic properties. One of the nanoparticles with zero H_c have $M_s \approx 35$ emu/g, and the others show $H_c \approx 17$ Oe and $M_s \approx 40$ emu/g. The M_s of sample B1 (50.8 emu/g) is higher than the values of the superparamagnetic $NiFe_2O_4$ nanoparticles in the studies mentioned above. d_{VSM} is calculated as 8.0 ± 0.4, 6.9 ± 0.6, 7.3 ± 0.5 and 7.4 ± 0.5 nm for B1, B2, B3 and B4, respectively. It can be concluded that the reaction temperature of the hydrothermal process is slightly effective on the properties of the $NiFe_2O_4$ nanoparticles.

The reaction time of the hydrothermal process was changed from 10 to 80 h, and the effect of the time on the properties of the nanoparticles was investigated. Figure 9

Fig. 11 TEM images of the nanoparticles synthesized at different times: **a** 10 h (*B5*) and **b** 80 h (*B9*) (*scale bar* is 20 nm)

shows the XRD patterns of the selected samples from B5 to B9 series. The patterns include (220), (311), (400), (422), (511), (440) and (533) peaks at $2\theta = 30.7°$, $36.0°$, $43.7°$, $54.2°$, $57.5°$, $63.2°$ and $75.3°$, respectively. Samples were crystallized in an inverse spinel structure of $NiFe_2O_4$. Crystal sizes, d_{XRD}, were calculated and are given in Table 2. d_{XRD} of samples B5, B7 and B9 is 7.9, 10.6 and 11.8 nm, respectively. It can be seen from the patterns in Fig. 9 that the width of the (311) peak slightly decreases and hence the crystal size increases as the reaction time increases.

Fig. 12 Magnetization curves of the nanoparticles synthesized at different times (*B5* 10 h, *B6* 20 h, *B7* 40 h, *B8* 60 h and *B9* 80 h). *Inset* shows the curves at ± 100 Oe
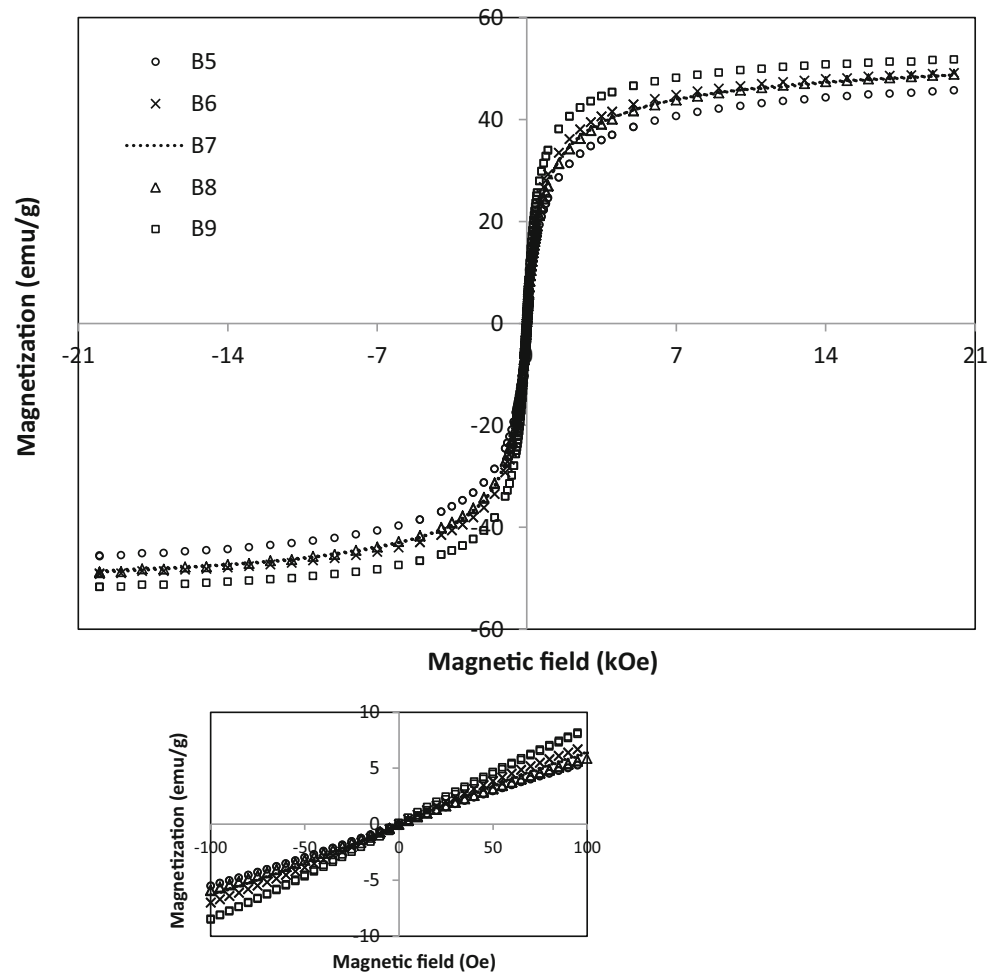
The FT-IR spectrum in Fig. 10 also confirms the NiFe$_2$O$_4$ nanoparticles by showing the bands around 397 and 598 cm^{-1} for all samples. TEM images of samples B5, B7 and B9 are given in Fig. 11, and d_{TEM} values of these samples are 6.6 ± 2.9, 10.1 ± 3.6 and 11.9 ± 3.9 nm, respectively. The increase in the physical particle sizes of the samples is consistent with the increase of crystal sizes. M_s of the samples increase from 45.6 to 51.7 emu/g as the reaction time increases from 10 to 80 h (Fig. 12). All samples except for B9 are superparamagnetic with zero H_c. Sample B9 has 2 Oe H_c. The d_{VSM} was also calculated for samples B5–B8 and is given in Table 2. Magnetic particle sizes of the samples are found to be around 7 nm. The d_{VSM} is also smaller than d_{TEM} and d_{XRD} for all samples since there might be a magnetically dead surface layer on the nanoparticles as reported in [27]. However, the similar trend of change is observed in the d_{XRD}, d_{TEM} and d_{VSM}. It is observed that the particle sizes of the samples having H_c are larger than those of the samples with zero H_c, indicating the limit of superparamagnetic size for NiFe$_2$O$_4$ nanoparticles. According to the d_{TEM} and d_{XRD} values of the samples

(Tables 1 and 2), it can be concluded that the limit of superparamagnetic particle size for our study is about 12 nm since NiFe$_2$O$_4$ nanoparticles show H_c.

4 Conclusions

Co-precipitation/hydrothermal synthesis was used to obtain NiFe$_2$O$_4$ nanoparticles. X-ray diffraction technique, Fourier transform infrared spectroscopy, transmission electron microscopy and vibrating sample magnetometer were used to characterize the nanoparticles. It was observed that the superparamagnetic NiFe$_2$O$_4$ nanoparticles can be synthesized by using the precursor synthesized at 80 °C. The effects of temperature and the time of the hydrothermal process on the structural and magnetic properties of the nanoparticles were investigated. The reaction temperature is slightly effective on the properties of the nanoparticles. However, the saturation magnetization (M_s) increases with the increase of the reaction time. Superparamagnetic NiFe$_2$O$_4$ nanoparticles with high M_s were obtained.

$NiFe_2O_4$ nanoparticles with zero H_c show high M_s of 50.8 emu/g which is close to the value of bulk nickel ferrite. d_{VSM} of the $NiFe_2O_4$ nanoparticles was also calculated to be 8.0 ± 0.4 nm.

References

1. Sohn, B.H., Cohen, R.E.: Processible optically transparent block copolymer films containing superparamagnetic iron oxide nanoclusters. Chem. Mater **9**, 264–269 (1997)

2. Hiergeist, R., Andrä, W., Buske, N., Hergt, R., Hilger, I., Richter, U., Keiser, W.: Application of magnetite ferrofluids for hyperthermia. J. Magn. Magn. Mater. **201**, 420–422 (1999)

3. Rossi, L.M., Costa, N.J.S., Silvia, F.P., Wojcieszak, R.: Magnetic nanomaterials in catalysis: advanced catalysts for magnetic separation and beyond. Green Chem. **16**, 2906–2933 (2014)

4. Lee, H., Shao, H.P., Huang, Y.Q., Kwak, B.: Synthesis of MRI contrast agent by coating superparamagnetic iron oxide with chitosan. IEEE Trans. Magn. **41**(10), 4102–4104 (2005)

5. Mornet, S., Vasseur, S., Grasset, F., Veverka, P., Goglio, G., Demourgues, A., Portier, J., Pollert, E., Duguet, E.: Magnetic nanoparticle design for medical applications. Progress Solid State Chem. **34**, 237–247 (2006)

6. Jain, T.K., Morales, M.A., Sahoo, S.K., Leslie-Pelecky, D.L., Labhasetwar, V.: Iron oxide nanoparticles for sustained delivery of anticancer agents. Mol. Pharm. **2**(3), 194–205 (2005)

7. Mc Gill, S.L., Cuylear, C.L., Adolphi, N.L., Osiński, M., Symth, H.D.C.: Magnetically responsive nanoparticles for drug delivery applications using low magnetic field strengths. IEEE Trans. Magn. **8**(1), 33–42 (2009)

8. Albuquerque, A.S., Ardisson, J.D., Macedo, W.A.A., Lopez, J.L., Paniago, R., Persiano, A.I.C.: Structure and magnetic properties of nanostructured Ni-ferrite. J. Magn. Magn. Mater. **226-230**, 1379–1381 (2001)

9. Goldman, A.: Modern Ferrite Technology. Springer, New York (2006)

10. Ahmad, T., Bae, H., Iqbal, Y., Rhee, I., Hong, S., Chang, Y., Lee, J., Sohn, D.: Chitosan-coated nickel-ferrite nanoparticles as contrast agents in magnetic resonance imaging. J. Magn. Magn. Mater. **381**, 151–157 (2015)

11. Lu, A.-H., Salabas, E.L., Schüth, F.: Magnetic nanoparticles: Synthesis, protection, functionalization, and application. Angew. Chem. Int. Ed. **46**, 1222–1244 (2007)

12. Mohapatra, M., Anand, S.: Synthesis and applications of nanostructured iron oxides/hydroxides—a review. Int. J. Eng. Sci. Technol. **2**(8), 127–146 (2010)

13. Harivardhan, R.L., Arias, J.L., Nicolas, J., Couvreur, P.: Magnetic nanoparticles: Design and characterization, toxicity and biocompatibility. Pharma. Biomed. Appl. Chem. Rev. **112**, 5818–5878 (2012)

14. Wang, J., Ren, F., Yi, R., Yan, A., Qiua, G., Liu, X.: Solvothermal synthesis and magnetic properties of size-controlled nickel ferrite nanoparticles. J. Alloys Compounds **479**, 791–796 (2009)

15. Ati, A.A., Othaman, Z., Samavati, A.: Influence of cobalt on structural and magnetic properties of nickel ferrite nanoparticles. J. Molecul. Struct. **1052**, 177–182 (2013)

16. Li, J., Lin, Y., Liu, X., Zhang, Q., Miao, H., Zhang, T., Wen, B.: The study of transition on $NiFe_2O_4$ nanoparticles prepared by co-precipitation/calcination. Phase Trans. **84**, 49–57 (2011)

17. Barreto, A.C.H., Santiago, V.R., Freire, R.M., Mazzetto, S.E., Sasaki, J.M., Vasconcelos, I.F., Denardin, J.C., Mele, G., Carbone, L., Fechine, P.B.A.: Grain size control of the magnetic nanoparticles by solid state route modification. J. Mater. Eng. Perform. **22**(7), 2073–2079 (2013)

18. Nejati, K., Zabihi, R.: Preparation and magnetic properties of nano size nickel ferrite particles using hydrothermal method. Chem. Central J. **6**, 23 (2012)

19. Shi, Y., Ding, J., Liu, X., Wang, J.: $NiFe_2O_4$ ultrafine particles prepared by co-precipitation/mechanical alloying. J. Magn. Magn. Mater. **205**, 249–254 (1999)

20. Laurent, S., Forge, D., Port, M., Roch, A., Robic, C., Vander Elst, L., Muller, R.N.: Magnetic iron oxide nanoparticles: Synthesis, stabilization, vectorization, physicochemical characterizations, and biological applications. Chem. Rev. **108**, 2064–2110 (2008)

21. Kahani, S.A., Jafari, M.: A new method for preparation of magnetite from iron oxyhydroxide or iron oxide and ferrous salt in aqueous solution. J. Magn. Magn. Mater. **321**, 1951–1954 (2009)

22. Cullity, B.D.: Elements of X-ray Diffraction. Addison-Wesley, USA (1978)

23. Lumina, S.M.M., Blessi, S., Pauline, S.: Effect of copper substitution on the structural, morphological and magnetic properties of nickel ferrites. Int. J. Res. (IJR) **1**(8), 1051–1054 (2014)

24. Sarkar, S., Mondal, A., Deyb, K., Ray, R.: Magnetic memory in nanocrystalline a-Fe2O3 embedded in reduced graphene oxide. RSC Adv. **5**, 81260–81265 (2015)

25. Maensiri, S., Masingboon, C., Boonchomb, B., Seraphin, S.: A simple route to synthesize nickel ferrite ($NiFe_2O_4$) nanoparticles using egg white. Scripta Materialia **56**, 797–800 (2007)

26. Morales, M.P., Veintemillas-Verdaguer, S., Montero, M.I., Serna, C.J., Roig, A., Casas, Ll., Martinez, B., Sandiumenge, F.: Surface and internal spin canting in γ-Fe_2O_3 nanoparticles. Chem. Mater. **11**, 3058–3064 (1999)

27. Liebermann, L., Clinton, J., Edwards, D.M., Mathon, J.: Dead layers in ferromagnetic transition metals. Phys. Rev. Lett. **25**, 232–235 (1970)